Am J Physiol Endocrinol Metab 299: E384–E393, 2010.
First published June 8, 2010; doi:10.1152/ajpendo.00226.2010.

FATP2 is a hepatic fatty acid transporter and peroxisomal very long-chain acyl-CoA synthetase

Alaric Falcon,[1]* Holger Doege,[2,3]* Amy Fluitt,[1] Bernice Tsang,[3] Nicki Watson,[5] Mark A. Kay,[4] and Andreas Stahl[1]

[1]*Department of Nutritional Sciences and Toxicology, University of California Berkeley, Berkeley; Departments of* [2]*GI/Hepatology and* [4]*Pediatrics and Genetics, Stanford University School of Medicine, Stanford;* [3]*Palo Alto Medical Foundation Research Institute, Palo Alto, California; and* [5]*Whitehead Institute for Biomedical Research, Cambridge, Massachusetts*

Submitted 15 April 2010; accepted in final form 3 June 2010

Falcon A, Doege H, Fluitt A, Tsang B, Watson N, Kay MA, Stahl A. FATP2 is a hepatic fatty acid transporter and peroxisomal very long-chain acyl-CoA synthetase. *Am J Physiol Endocrinol Metab* 299: E384–E393, 2010. First published June 8, 2010; doi:10.1152/ajpendo.00226.2010.—Fatty acid transport protein (FATP)2, a member of the FATP family of fatty acid uptake mediators, has independently been identified as a hepatic peroxisomal very long-chain acyl-CoA synthetase (VLACS). Here we address whether FATP2 is *1*) a peroxisomal enzyme, *2*) a plasma membrane-associated long-chain fatty acid (LCFA) transporter, or *3*) a multifunctional protein. We found that, in mouse livers, only a minor fraction of FATP2 localizes to peroxisomes, where it contributes to approximately half of the peroxisomal VLACS activity. However, total hepatic (V)LACS activity was not significantly affected by loss of FATP2, while LCFA uptake was reduced by 40%, indicating a more prominent role in hepatic LCFA uptake. This suggests FATP2 as a potential target for a therapeutic intervention of hepatosteatosis. Adeno-associated virus 8-based short hairpin RNA expression vectors were used to achieve liver-specific FATP2 knockdown, which significantly reduced hepatosteatosis in the face of continued high-fat feeding, concomitant with improvements in liver physiology, fasting glucose, and insulin levels. Based on our findings, we propose a model in which FATP2 is a multifunctional protein that shows subcellular localization-dependent activity and is a major contributor to peroxisomal (V)LACS activity and hepatic fatty acid uptake, suggesting FATP2 as a potential novel target for the treatment of nonalcoholic fatty liver disease.

nonalcoholic fatty liver disease

FATTY ACID TRANSPORT PROTEIN (FATP)2 has been suggested to perform various functions. It was first discovered as a peroxisomal very long-chain acyl-CoA synthetase (VLACS) (38). Independently, FATP2 was identified as a member of the FATP family in the context of protein-mediated long-chain fatty acid (LCFA) uptake (18). In addition to its function in lipid metabolism, overexpression of FATP2 in COS-1 cells was later shown to increase bile CoA ligase activity (23). Thus FATP2 has the potential to impact several important pathways of lipid and bile metabolism, but it remains unclear if, and to what degree, hepatic FATP2 fulfills all these suggested functions in vivo.

FATP2 and FATP5 are the two major FATPs in the liver (2, 18, 33, 37). As the peroxisomal liver VLACS, FATP2 has the potential to contribute to the etiology of X-linked adrenoleukodystrophy (X-ALD) (38). X-ALD is a progressive neurodegenerative disease, characterized by an accumulation of very long-chain fatty acids (VLCFA), particularly in the brain and adrenal glands (24). While initially the X-ALD defect was thought to involve a peroxisomal VLACS (15), positional cloning identified ATP-binding cassette (ABC) protein D1 (ABCD1) as the adrenoleukodystrophy protein (ALDP) (25). A dysfunctional FATP2 was thought to result in lowered peroxisomal (V)LCFA β-oxidation, leading to accumulation of substrates. FATP2 knockout mice demonstrated that deletion of FATP2 indeed led to reduced peroxisomal VLACS activity and peroxisomal LCFA β-oxidation. However, loss of FATP2 did not cause an X-ALD phenotype, nor did it enhance disease progression in ALDP knockout mice (16).

Another enzymatic function that has been suggested to be linked to hepatic FATP2 and FATP5 is bile CoA ligase activity (23, 36). CoA synthetases are required for bile acid conjugation, as well as the side chain shortening steps of bile synthesis. During the latter reaction, the C_{27} bile intermediates 3α,7α-dihydroxycholestanoic acid (DHCA) and 3α,7α,12α-trihydroxycholestanoic acid (THCA) are esterified with CoA prior to peroxisomal β-oxidation and conversion to C_{24} chenodeoxycholate and cholate, respectively (28). Earlier, in FATP5 knockout mice, we demonstrated impairment of primary and secondary bile acid reconjugation without effect on bile acid de novo synthesis (19), indicating that FATP5 is not required for DHCA/THCA activation. Furthermore, side chain shortening is thought to occur in peroxisomes, which do not contain FATP5 (6, 9). This led to the proposal that FATP2 is solely involved in side chain shortening of cholesterol during bile synthesis (19). Thus its loss should result in dysfunctional de novo bile synthesis and decreased total bile acid levels. However, this prediction has not been validated in FATP2 knockout mice or other in vivo loss-of-function systems.

The enhanced uptake of free fatty acid (FFA) is a well-documented and evolutionarily conserved function of the FATP family (18, 32, 33). It is a saturable process that can be inhibited by small molecules (3), and FFA transport can be discerned from other functions by point mutations within FATP (30, 42). While the exact mechanism of transport has remained elusive, vectorial acylation has been proposed as the method for FATP-mediated FFA transport. This model suggests that intracellular LCFA activation allows for sequestering and/or breakdown of fatty acids to maintain a concentration gradient, which leads to LCFA uptake (43). Although much debate has centered on the transport mechanism, the link between FATP function and cellular LCFA

* A. Falcon and H. Doege contributed equally to this work.

Address for reprint requests and other correspondence: A. Stahl, 119 Morgan Hall, UC Berkeley, Berkeley, CA 94720 (e-mail: AStahl@Berkeley.edu).

uptake has been well established in mouse model systems (8). While FATP3 and FATP4 are expressed only at low levels in the liver, FATP2 and FATP5 are expressed at the highest levels (2, 18, 33, 37). A ^{14}C tracer in vivo has shown a >40% decrease in LCFA uptake from isolated hepatocytes and a reduced absorption of LCFAs in the liver in FATP5 knockouts (6). In addition, by showing that silencing of hepatic FATP5 in a diet-induced nonalcoholic fatty liver disease (NAFLD) model resulted in reversal of hepatosteatosis, our group demonstrated that FATP5-dependent hepatic LCFA uptake contributes to NAFLD upon lipid oversupply (7). While the role of FATP2 in hepatosteatosis has not been addressed, one would expect that loss of FATP2 function would result in an improvement of NAFLD similar to that observed following knockdown of FATP5.

To delineate the diverse roles of FATP2 in vivo, we determined its subcellular localization in hepatocytes and established adeno-associated virus (AAV)-based knockdown strategies to elucidate the impact of FATP2 inhibition on liver (V)LACS activity, LCFA uptake, and hepatosteatosis.

MATERIALS AND METHODS

Antibodies and reagents. BODIPY fatty acid (C_1-BODIPY$^{500/512}$-C_{12}) and Dynabeads MyOne streptavidin T1 magnetic beads were purchased from Invitrogen (Carlsbad, CA). [^{14}C]oleic acid was obtained from ARC (St. Louis, MO). Polyclonal antisera against the COOH termini of FATP2, FATP4, and FATP5 were raised as described previously (8, 34). Anti-PMP70 was a gift from Eveline Baumgart-Vogt (1). Anti-β-tubulin, anti-catalase, and biotinylated anti-PMP70 antibodies were purchased from BD Biosciences (San Jose, CA), BD Transduction Laboratories (San Jose, CA), and Abcam (Cambridge, MA), respectively. All other chemicals were obtained from Sigma (St. Louis, MO).

Peroxisome purification. Peroxisomes were isolated according to a modification of a previously described protocol (21). Briefly, 1 ml of ice-cold 250 mM sucrose, 10 mM MOPS (pH 7.4), 0.1 mM EDTA, 0.2 mM DTT, and protease inhibitor cocktail was added to 500 mg of liver. After 60 stokes of a Dounce homogenizer, the liver lysates were centrifuged at 1,000 *g* for 10 min. The supernatant was centrifuged at 5,000 *g* for 10 min. The resulting supernatant was mixed with prepared streptavidin magnetic beads. The beads were prepared as follows: 100 μl (1 mg) of beads were mixed with 500 μl of PBS; then the beads were washed three times for 30 min with PBS on a magnetic sorter, and the supernatant was removed. The beads were mixed with 10 μg of biotinylated anti-PMP70 and 500 μl of PBS with gentle rotation for 30 min at room temperature, washed three times with PBS, and mixed with 20 nmol of biotin and 500 μl of PBS with rotation for 30 min at room temperature. Finally, the beads were washed three times with PBS. Prepared beads in 500 μl of PBS and 500 μl of the supernatant from the liver homogenates were mixed with gentle rotation at 4°C for 1 h. Peroxisomes were isolated bound to magnetic beads after four washes with PBS.

Short hairpin RNA constructs. FATP2 short hairpin RNA (shRNA) sequences were created as suggested elsewhere (27) and did not have any homology with other mouse genes. In vitro experiments used the human H1 promoter in pSUPERIOR (OligoEngine, Seattle, WA) to express all shRNAs. All shRNAs had a loop sequence of 5′-TTCAAGAGA-3′ (targeting sequences are listed in Supplemental Fig. S1; Supplemental Material for this article is available online at the *AJP-Endocrinology and Metabolism* web site). Stabilized double-stranded AAV vectors were created, generated, purified, and titered as previously described (12).

Microscopy. A laser scanning confocal microscope (Zeiss, Oberkochen, Germany) was used for confocal microscopy. Slides were prepared by cryosectioning optimal cutting temperature compound-embedded tissues that were fixed with 2% paraformaldehyde. Sections were blocked for 30 min with 1% BSA, 10% FBS, 0.05% saponin, and 2% normal donkey serum in HBSS. Primary and secondary antibodies were diluted in the blocking solution and incubated for 1 h. Prolong Gold antifade reagent with 4′,6-diamidino-2-phenylindole (Invitrogen) was used to mount stained sections. Volumetric and colocalization analysis was completed with Imaris software (Bitplane, Zurich, Switzerland). Immunogold electron microscopy was performed as previously described on an electron microscope (model EM 410, Philips) (34). Liver histology was accomplished by using Masson's trichrome reagent and BODIPY$^{493/503}$ (Invitrogen) (6). The Brunt system for grading and staging of fatty livers was used to assess the liver morphology and hepatosteatosis (4).

Fatty acid uptake assays. All uptake assays were performed as previously described (6, 20, 34). Briefly, cells were incubated with prewarmed 200 μmol/l [^{14}C]palmitate, -oleate, -linoleate, or -octanoate bound to BSA at a 2:1 molar ratio in HBSS. An ice-cold solution of 0.1% BSA and 0.05% phloretin in HBSS was used to stop uptake. Cells were lysed with radioimmunoprecipitation assay buffer and assayed for radioactivity. As an alternative method, isolated hepatocytes or transfected HEK 293 cells (created using FuGENE 6, Roche, Palo Alto, CA) were used for fluorescein-activated cell sorting-based fluorescent uptake assays. Cells were washed and incubated for 30 s at 37°C with a prewarmed 0.1 μM BODIPY fatty acid and 0.1% essentially fatty acid-free BSA in HBSS. Uptake was halted with an ice-cold stop solution. Real-time uptake kinetic assays were carried out according to the manufacturer's instructions (Molecular Devices, Sunnyvale, CA).

LACS and VLACS assays. On the basis of previously described methods (39), the LACS and VLACS assays are similar to each other, and the differences are indicated with the VLACS changes in parentheses. The (V)LACS assays were completed by lysing mouse livers in 10 volumes of 300 mM sucrose-2 mM MOPS-NaOH (pH 7.4) with a Dounce homogenizer. The lysates were then diluted to 50–100 mg/ml (1–2 μg/ml), and 20 μl (10 μl) of diluted liver lysates were mixed with 180 μl (90 μl) of 150 mM Tris·HCl (pH 8.5), 200 μM CoA, 10 mM ATP, 10 mM $MgCl_2$, and 10 μM [^{14}C]oleate (10 μM lignocerate and 1 μM [^{3}H]lignocerate dissolved in 30 mg/ml α-cyclodextrin) at 37°C for 10 min. The reaction was terminated by addition of 150 μl (75 μl) of the above-described mixture to 750 μl (1,125 μl) of Dole's reagent [10:40:1 (vol/vol/vol) heptane-2-propanal-2 N sulfuric acid]. After centrifugation, the supernatant [650 μl (975 μl)] was washed three times with 350 μl (525 μl) of heptane and 190 μl (292.5 μl) of 400 mM MOPS-NaOH (pH 6.5), and the radioactivity of the lower phase was assayed.

Animal procedures. All animal studies were approved by the Palo Alto Medical Foundation Research Institute and the University of California Berkeley Institutional Animal Care and Use Committee. C57Bl6 mice (Jackson Laboratories, Bar Harbor, ME) were fed regular laboratory chow (no. 5P75, LABDiet, Richmond, IN), low-fat diet (no. D12450, Research Diets) containing 10% fat, or high-fat diet (no. D12492, Research Diets) containing 60% fat. Mice used in the knockdown studies received 3×10^{11} viral particles of stabilized double-stranded AAV8 in 250 μl of PBS or PBS alone via tail vein injections (26). Commercially available kits were used to determine FFA (Wako Chemicals, Richmond, VA), triglycerides (TG), total bile, cholesterol (Sigma Diagnostics, St. Louis, MO), β-hydroxybutyrate, alanine aminotransferase, aspartate aminotransferase, bilirubin (Stanbio Laboratory, Borne, TX), glucose (Themo Electron), and insulin (ALPCO Diagnostic, Windham, NH) from serum samples collected by retroorbital bleeding of each mouse. For glucose tolerance tests, mice were fasted overnight and then injected with glucose (2 mg/kg body wt

ip). Similarly, insulin tolerance tests were accomplished by insulin injection (0.75 U/kg body wt). Whole blood was used to measure glucose with a glucometer (Bayer). For measurement of fatty acid absorption, 250 μl of olive oil and 3.5 μCi of [^{14}C]oleic acid were delivered via gavage, and blood samples were taken through orbital eye bleeds at 0, 30, 60, 120, and 240 min. Radioactivity of serum was assayed by scintillation counting.

Hepatocyte preparation. Mouse livers were cannulated through the portal vein, and an incision was made in the lower vena cava. Following the manufacturer's instructions (Invitrogen), perfusion and digestion media were used to perfuse the livers and isolate hepatocytes.

Tissue lipid analysis. Tissues were ground in liquid nitrogen and extracted using the method of Folch et al. (10). TG was determined using the Sigma Diagnostics kit.

Statistical analysis. Statistical analysis was carried out by Student's *t*-test and analysis of variance; $P < 0.05$ was considered significant.

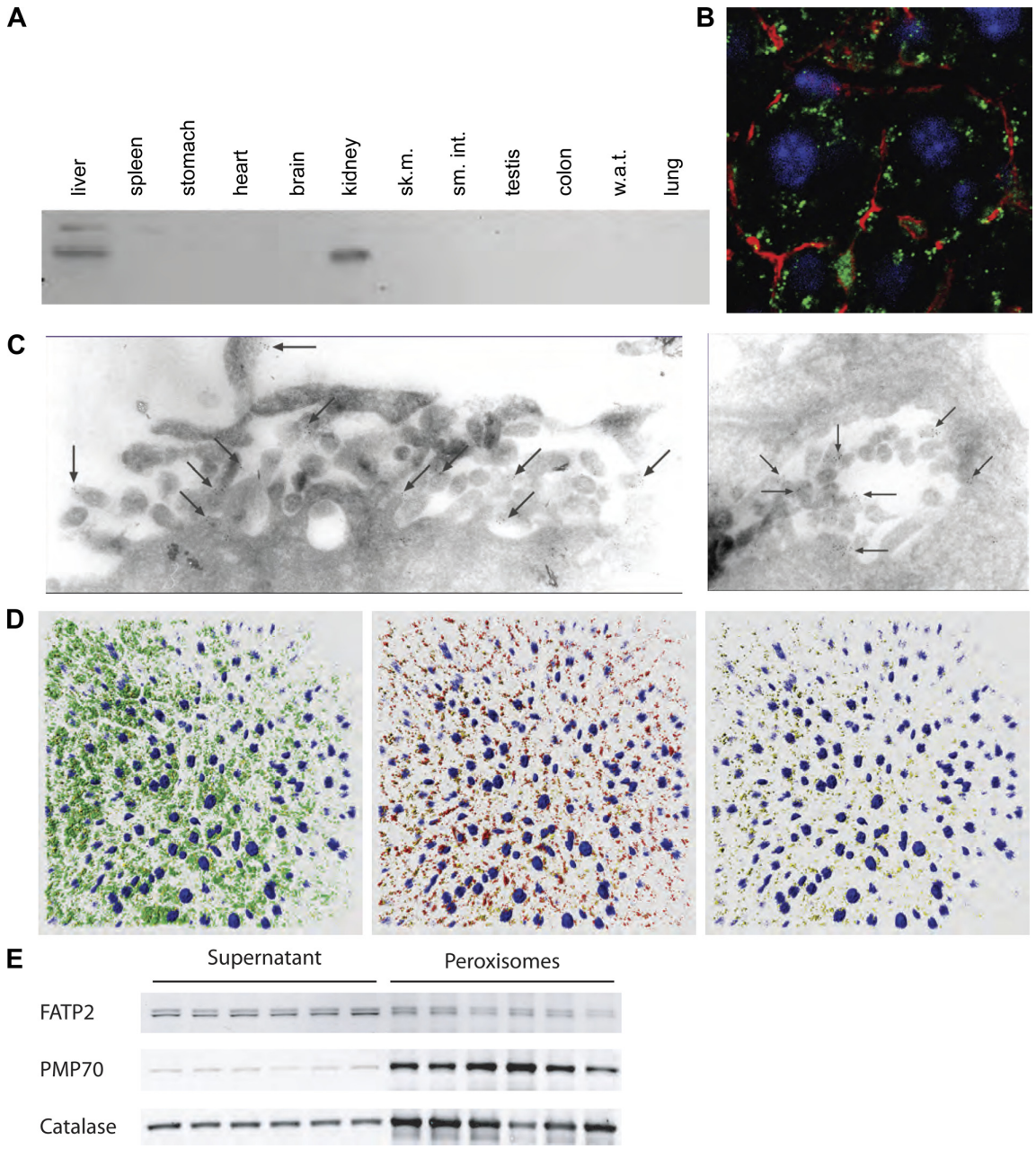

Fig. 1. *A*: Western blot of tissue lysates probed with anti-fatty acid transport protein (FATP)2. sk.m, skeletal muscle; sm.int, small intestine; wat, white adipose tissue. *B*: confocal immunofluorescent microscopy image of mouse liver sections stained with anti-FATP2 (green channel) and actin-binding phalloidin (red channel). *C*: immunoelectron microscopy image of mouse liver sections treated with anti-FATP2 antibodies bound to gold particles (arrows) in the space of Disse (*left*) and bile canaliculi (*right*). *D*: 3-dimensional reconstructions of serial confocal scans through mouse liver sections stained with 4′,6-diamidino-2-phenylindole (blue channel), anti-PMP70 (green channel), and anti-FATP2 (red channel) and colocalization of PMP70 and FATP2 (yellow). *E*: immunoisolated peroxisomes and supernatant after the first magnetic sorting and blotting with anti-FATP2, anti-PMP70, or anti-catalase.

RESULTS

The majority of FATP2 does not localize to peroxisomes. FATP2 was originally identified as a peroxisomal VLACS (38) but also has been characterized as a member of the FATP family (18), which is thought to enhance LCFA membrane traversal. These two functions presumably require different subcellular localizations: to peroxisomes and the plasma membrane, respectively. To assess FATP2 localization and expression patterns, using the unique COOH terminus of FATP2 as antigen to avoid cross-reactivity with other FATP family members, we raised a FATP2-specific polyclonal serum in rabbit. On the basis of Western blots with lysates from HEK 293 cells transiently transfected with different FATPs, the antiserum reacted strongly with FATP2, but not with any of the other FATPs (data not shown). The anti-FATP2 serum detects a ~70-kDa protein in liver and kidney lysates (Fig. 1*A*). Confocal immunofluorescent microscopy of mouse liver sections shows the FATP2 protein to be predominantly localized in a punctuate pattern inside the cytoplasm and along the plasma membrane of hepatocytes, compared with the staining of actin (Fig. 1*B*). Immunoelectron microscopy revealed FATP2 to be localized to basal and apical microvilli in the space of Disse and in bile canaliculi, respectively (Fig. 1*C*). To assess how much of the total hepatic FATP2 pool resides in peroxisomes, we performed microscopic and biochemical assays. Three-dimensional reconstructions of serial confocal scans through liver sections stained for the peroxisome marker PMP70 and FATP2 were utilized to calculate the overlap between the two proteins in a larger spatial volume using the Imaris software package (Fig. 1*D*). An average of 8% of the FATP2 signal overlapped with PMP70. As an alternative approach, we used PMP70-based immunoisolation of peroxisomes (21) to minimize contamination with other organelle fractions. This technique used streptavidin-coated magnetic beads that were bound with biotin-conjugated anti-PMP70 antibodies. After magnetic sorting with several washes, an enriched population of PMP70-expressing organelles was obtained. To account for animal-to-animal and experimental variations, six peroxisome isolations from the livers of male C57Bl6 mice were completed in parallel. Western blots for the nonperoxisomal membrane fraction (supernatant) and peroxisomes showed an average 57-fold enrichment for PMP70 but no enrichment for FATP2 (Fig. 1*E*). In contrast, catalase, which in mouse liver is found in peroxisomal and nonperoxisomal fractions such as Golgi and endoplasmic reticulum (41), was enriched by a factor of 2.4. After normalization to protein concentration and volume of resuspension, it was calculated that 2% of total hepatic FATP2 resides in PMP70-containing peroxisomes. Thus the majority of hepatic FATP2 does not localize to peroxisomes.

FATP2 mediates LCFA uptake. Initial experiments with stable HEK 293 cells overexpressing human FATP2 confirmed that the substrate specificities of FATP2 are comparable to those of other FATPs (34), i.e., enhanced uptake of LCFAs such as palmitate, oleate, and linoleate, with no effect on medium-chain fatty acid (octanoate) uptake (data not shown). The extent of the increase in uptake of a fluorescently labeled LCFA (C_1-BODIPY-C_{12}, BODIPY-LCFA) observed with FATP2 expression was similar to that observed with expression of FATP1 or FATP5 in the same HEK 293 cells and under the same selection conditions (Fig. 2*A*). These assays were

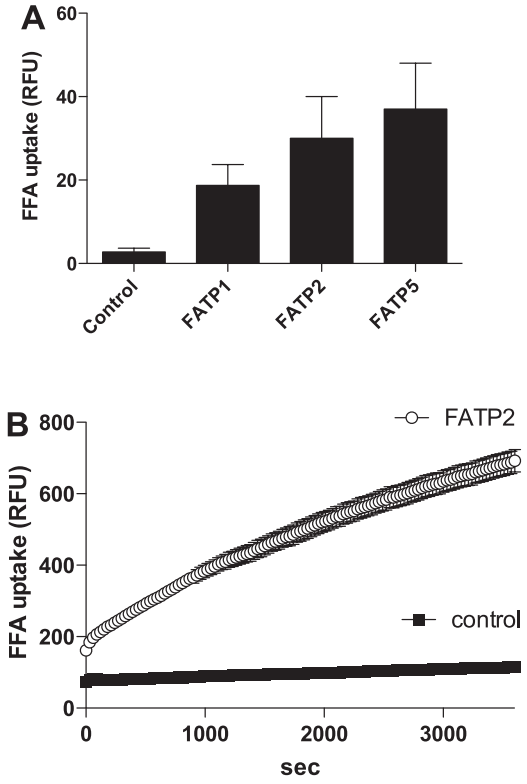

Fig. 2. Stable HEK 293 cells that overexpressed human FATP1, human FATP2, human FATP5, or control vector were used for a variety of uptake experiments. *A*: fluorescent-labeled fatty acid (C_1-BODIPY-C_{12}) measurement of fatty acid uptake in control, FATP1, FATP2, and FATP5 cell lines. FFA, free fatty acid; RFU, relative fluorescence units. *B*: quencher-based assay of fatty acid uptake kinetics in FATP2 and control cell lines.

determined by flow cytometer-based end-point assays for fatty acid uptake. Using a quencher-based fatty acid uptake assay (20), we were able to compare uptake kinetics of FATP2-transfected with vector-transfected control HEK 293 cells. FATP2 expression greatly enhanced BODIPY-LCFA uptake over control cells, and initial uptake rates were linear over the first 1,000 s with a 10 μM substrate concentration (Fig. 2*B*).

In vitro and in vivo knockdown of FATP2. To explore the contribution of FATP2 to hepatic lipid metabolism in vivo, we took advantage of an AAV-based shRNA technology, which we recently used to silence hepatic FATP5 expression (7). We first established a FATP2-shRNA cotransfection assay that was used to identify functional FATP2-specific shRNA sequences. Two (FATP2-6 and FATP2-7) of the nine screened shRNA constructs were able to completely suppress FATP2-mediated fatty acid uptake (Fig. 3*B*), as well as FATP2 protein expression (Fig. 3*A*), in our in vitro systems. Based on FATP2-6 and FATP2-7, we generated two AAV-shRNA expression constructs to target FATP2, as well as a scrambled (SCR) shRNA sequence control vector, as previously reported for FATP5 (7). Western blots of liver lysates at 1 wk following a tail vein injection of AAV-shRNA particles showed that AAV-FATP2-6, but not AAV-FATP2-7, was able to mediate a robust knockdown of hepatic FATP2 in vivo (Fig. 3*C*). We previously reported similar

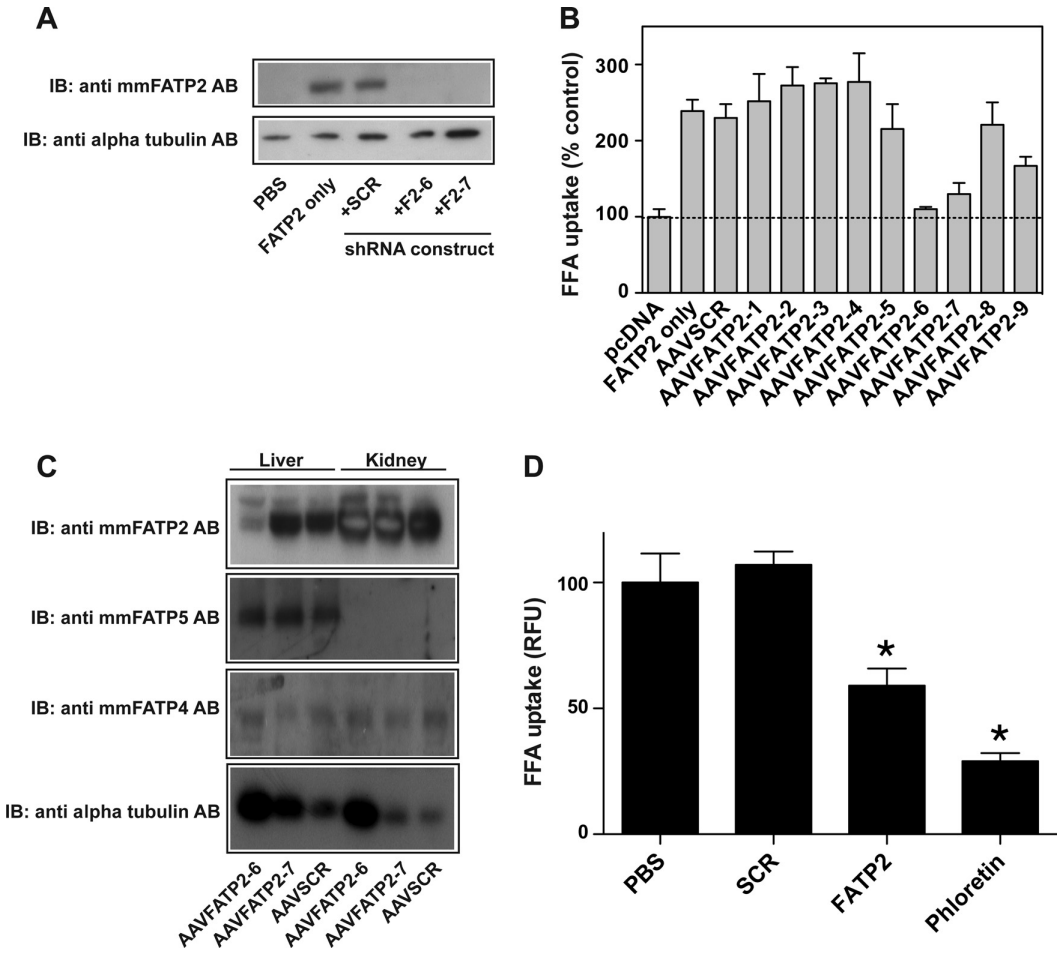

Fig. 3. In vitro (*A* and *B*) and in vivo (*C* and *D*) experiments tested knockdown effects of control and FATP2-short hairpin RNA (shRNA) sequences. *A*: Western blots of transfections with FATP2 expression plasmid (FATP2 only) or cotransfections with FATP2 expression plasmid and 1 of 3 shRNA constructs [scrambled (SCR), F2-6, F2-7]. IB, immunoblot; mmFATP2, *Mus musculus* FATP2. *B*: fluorescent fatty acid uptake assay of transfections with negative control pcDNA3.1 (pcDNA), transfections with FATP2 expression plasmid (FATP2 only), or cotransfections with FATP2 expression plasmid and 1 of 9 shRNA constructs [adeno-associated virus (AAV)-SCR and AAV-FATP2-1 to AAV-FATP2-9]. *C*: Western blots of liver and kidney lysates from AAV-shRNA-treated mice. *D*: fluorescent fatty acid uptake assay with isolated hepatocytes from PBS-, AAV-FATP2-6-, or AAV-SCR-injected mice. Phloretin-treated hepatocytes were harvested from normal C57Bl6 mice. $*P < 0.05$.

observations (6, 8) but failed to provide an explanation for this unpredictable translation from functional in vitro to efficient in vivo sequences. Importantly, knockdown of hepatic FATP2 did not alter FATP2 expression in the kidney or affect the expression levels of FATP5 in the liver (Fig. 3*C*), demonstrating organ and target specificity. AAV-FATP2-6 was used for all subsequent experiments. To demonstrate the impact of loss of FATP2 function on hepatic fatty acid uptake, we performed fluorescein-activated cell sorting-based fatty acid uptake assays with isolated hepatocytes (7) 1 wk following the injection of PBS, control virus, or FATP2-specific virus. Comparison of fatty acid uptake with control hepatocytes treated with phloretin, a nonspecific inhibitor of protein-mediated uptake processes at the plasma membrane, showed a robust (~40%) reduction of fatty acid uptake by hepatocytes from FATP2 knockdown mice (Fig. 3*D*). To investigate the impact on total and peroxisomal long-chain acyl-CoA synthetase (LACS) and VLACS activity, we performed enzyme assays using palmitate and lignocerate as respective substrates. At 10 days following injection of scrambled AAV-shRNA (AAV-shRNA-SCR) or AAV-shRNA-FATP2 particles, livers were harvested, and loss of FATP2 (>92%) was confirmed by Western blotting (Fig. 4*A*). Loss of FATP2 did not significantly affect LACS or VLACS activity in total liver lysates (Fig. 4, *B* and *C*), indicating that the contribution of FATP2 to total (V)LACS activity is minor or that increased expression of other microsomal enzymes is able to compensate. In contrast, LACS and VLACS activity in immunopurified peroxisomes was reduced by 59% and 51%, respectively (Fig. 4, *D* and *E*).

Inhibition of hepatic FATP2 improves hepatosteatosis and glucose homeostasis. Because the treatment of human liver disorders is more informed by the reversal than the prevention of hepatosteatosis, we designed an experiment in which all animals were initially fed a high-fat diet for 6 wk, which is sufficient to cause significant hepatosteatosis (7), injected with mock PBS, AAV-control, or AAV-FATP2, and fed a high-fat diet for an

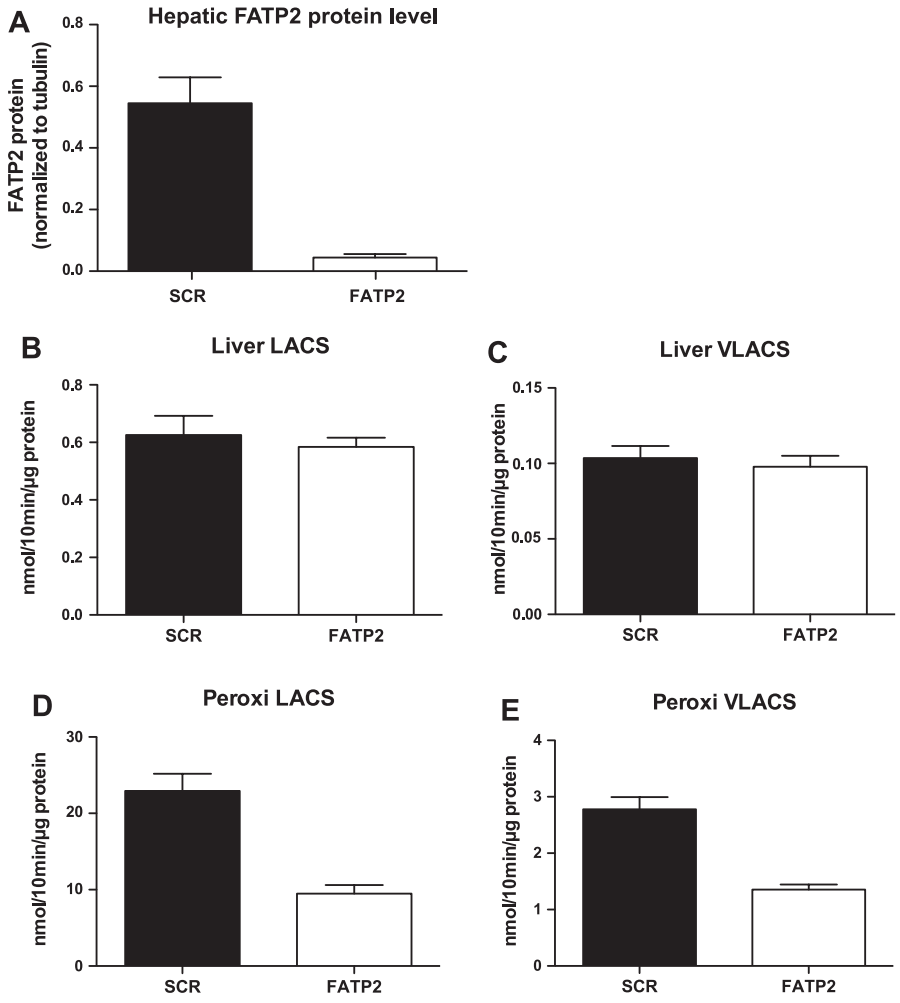

Fig. 4. *A*: FATP2 knockdown in liver of AAV-control-SCR or AAV-shRNA-FATP2 mice. *B* and *C*: palmitate and lignocerate assay of total liver long-chain and very long-chain acyl-CoA synthetase (LACS and VLACS) levels in AAV-control-SCR- and AAV-shRNA-FATP2-injected mice. *D* and *E*: palmitate and lignocerate assay of immunoisolated peroxisomal LACS and VLACS levels.

additional 6 wk. Alternatively, animals were fed a matched low-fat diet over the 12 wk of the experiment and received injections at *week 6*, as outlined for the high-fat diet group. A single injection of FATP2-specific AAV-shRNA particles at *week 6* was sufficient to cause a complete loss of FATP2 protein at the end of the 12-wk study without affecting hepatic FATP5 or FATP4 expression (Fig. 5*A*). Total liver TG content was marginally lower in FATP2 knockdown mice fed a low-fat diet than control mice (Fig. 5*B*). High-fat feeding markedly increased hepatic lipid content in all groups; however, loss of FATP2 function led to a significant reduction in liver TG (Fig. 5*B*). By contrast, levels of hepatic free and esterified cholesterol were not affected by FATP2 knockdown (Fig. 5*C*). Consistent with the unaffected expression of FATP2 in kidney, TG content in this organ was unchanged following FATP2 knockdown (Fig. 5*D*), while lipid content in skeletal and cardiac muscle was slightly increased (data not shown). The reduction in hepatosteatosis following FATP2 knockdown was also clearly detectable by histological examination of liver sections. Masson's trichrome staining of control livers from animals fed a high-fat diet showed clear signs of macrovesicular steatosis without cirrhosis, indicating that progression to nonalcoholic hepatosteatosis did not occur. The control liver also had significant lipid deposition, as detected by staining with BODIPY$^{493/503}$ (Fig. 5*E*). Loss of FATP2 caused a clear improvement in morphology and neutral lipid content (Fig. 5*E*), indicating a significant reversal of established hepatosteatosis.

While body weight and food consumption of FATP2 animals fed low- or high-fat diets were not significantly different from AAV-SCR controls (Fig. 6, *A* and *B*), fasting glucose levels showed a marked improvement following loss of FATP2. After 6 wk of high-fat feeding, serum glucose levels were clearly elevated in all mice prior to AAV injection (Fig. 6*C*). Importantly, 4 wk following AAV-FATP2 injection, serum glucose levels were significantly lower in FATP2 knockdown animals than AAV-SCR controls and remained lower throughout the rest of the study (Fig. 6*C*), despite the animals' identical weight and food consumption. Glucose tolerance tests in high-fat-fed animals also demonstrated significantly lower values for FATP2 knockdown animals (Fig. 6*D*). However, when corrected for lower initial glucose values, areas under the curve were identical for AAV-SCR control and AAV-FATP2 animals (19,724 and 19,635, respectively). This indicated that glucose disposal, which is primarily a function of skeletal muscle and adipose tissue, was unchanged following inhibition of hepatic

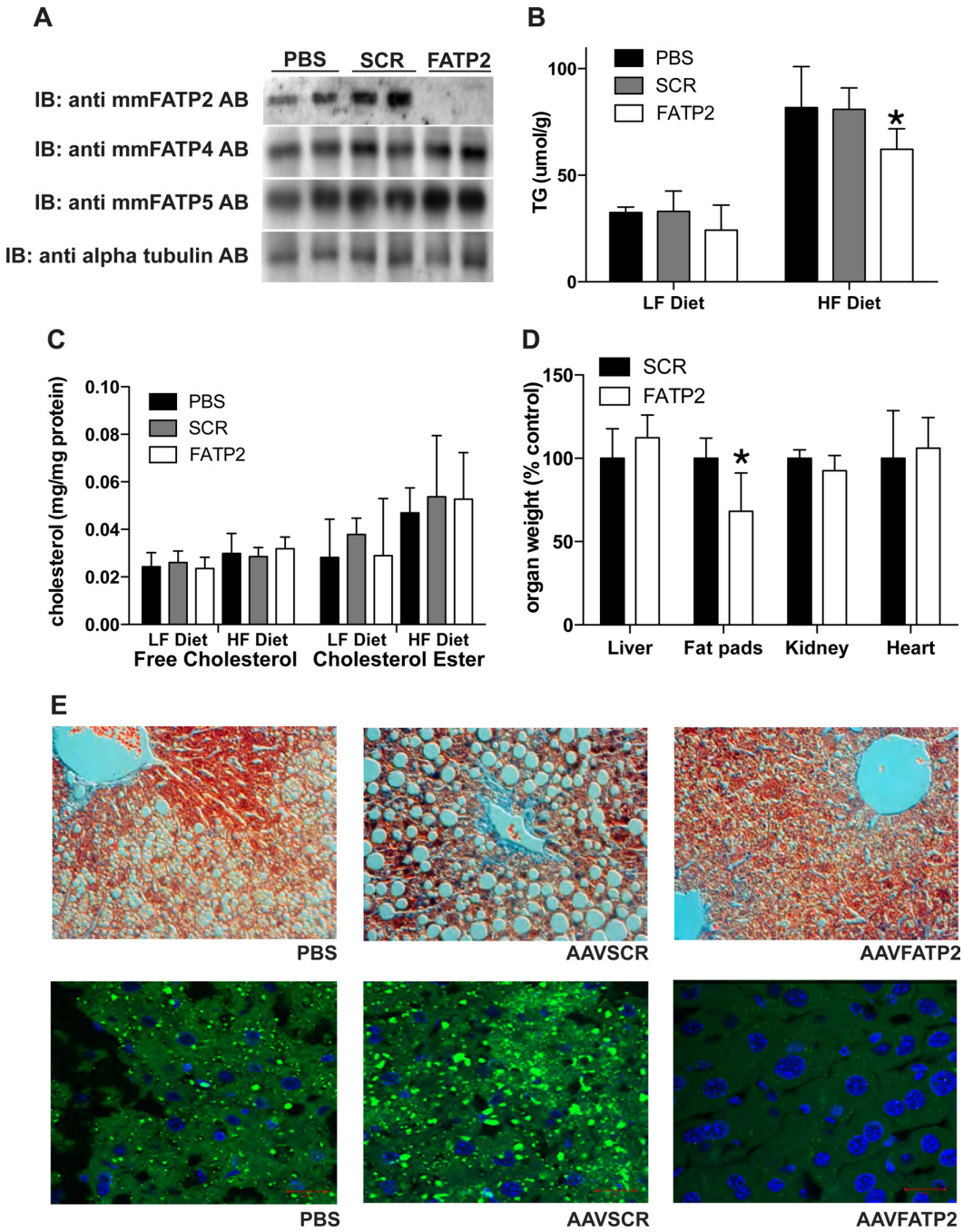

Fig. 5. At the end of the 12-wk diet study, PBS-, AAV-control-SCR-, and AAV-shRNA-FATP2-treated mice were analyzed by a variety of tests. *A*: Western blots for FATP2, FATP4, FATP5, and α-tubulin in liver. *B*: total hepatic triglycerides (TG) for mice fed low-fat (LF) and high-fat (HF) diets. *C*: serum free cholesterol and cholesterol esters for mice fed low- and high-fat diets. *D*: weight of liver, fat pads, kidneys, and heart. *E*: histological sections of mouse liver stained with Masson's trichrome (*top*) or BODIPY$^{493/503}$ (*bottom*). *$P < 0.05$.

FATP2. A further indication of improved insulin sensitivity following loss of FATP2 in high-fat-fed animals was the reduction in fasting insulin levels (Table 1) from 1.21 to 0.95 ng/ml. The lower fasting serum insulin and glucose levels led to a significant improvement in the homeostasis model assessment of insulin resistance score from 9.3 for AAV-SCR-injected animals to 6.4 for AAV-FATP2-injected animals. Fasted serum lipid parameters, including total serum TG, FFAs, and cholesterol, were unaffected by loss of hepatic FATP2 (Table 1), but fatty acid clearance, measured by a [^{14}C]fatty acid tracer, was slowed in this experimental setting (see Supplemental Fig. S2). Interestingly, [^{14}C]fatty acid absorption (see Supplemental Fig. S2) and total serum bile levels were not reduced in FATP2 knockdown animals, despite the suggested role of FATP2 in bile synthesis (23).

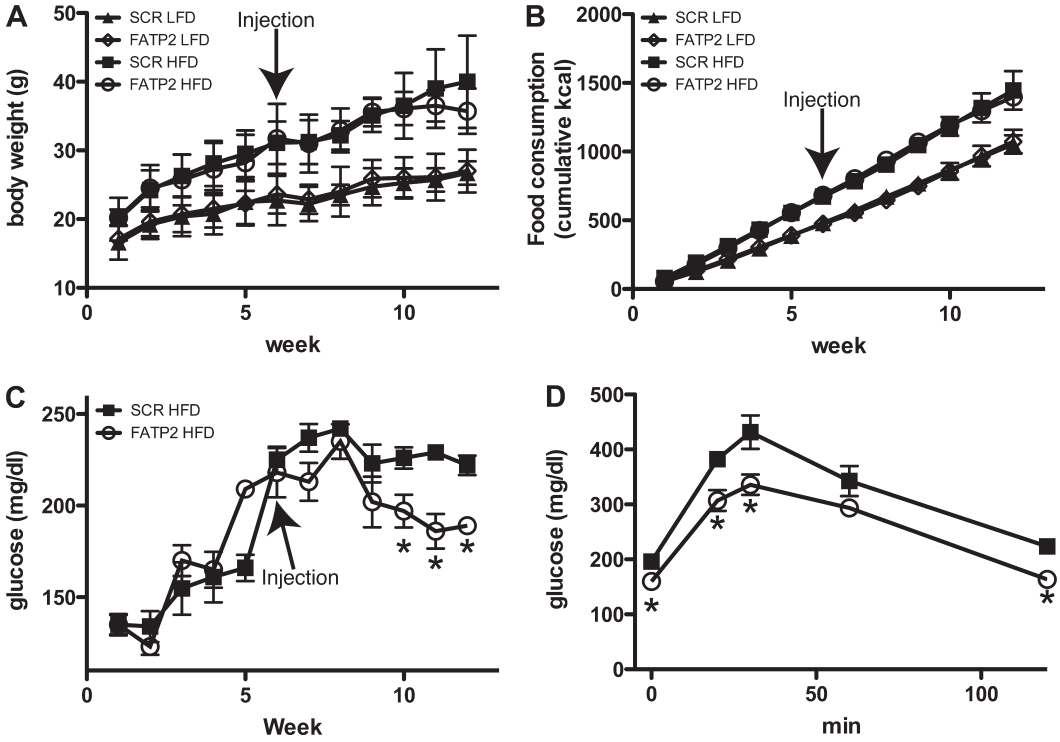

Fig. 6. Weekly measurements of body weight (*A*), food consumption (*B*), and fasting glucose (*C*) in control and FATP2 knockdown animals fed low- and high-fat diets (LFD and HFD). *D*: results from glucose tolerance tests administered to mice in *week 12*. *$P < 0.05$.

DISCUSSION

FATP2 is a member of the FATP family and is predominantly expressed in liver and kidney. Focusing on lipid metabolism, hepatic FATP2 has been ascribed a number of functions, including peroxisomal VLACS and plasma membrane fatty acid transport. However, the relative contribution of FATP2 to either function and the physiological consequences of loss of hepatic FATP2 for liver lipid metabolism have remained unclear. Here we investigated the subcellular distribution of FATP2 and utilized an AAV-shRNA-based strategy to determine the impact of loss of liver FATP2 function on VLACS activity, hepatic lipid metabolism, and insulin sensitivity.

Table 1. *Serum parameters for high-fat-fed C57Bl6/J mice injected with AAV-control-SCR and AAV-shRNA-FATP2*

	AAV-Control-SCR	AAV-shRNA-FATP2	*P*
Glucose, mg/dl	131 ± 8.2	114 ± 12.4*	0.01
Insulin, ng/ml	1.21 ± 0.1	0.95 ± 0.281*	0.03
HOMA-IR	9.3 ± 0.9	6.4 ± 1.9*	0.02
FFA, mM	1.85 ± 0.19	1.87 ± 0.13	0.81
TG, mg/dl	189 ± 18.7	174 ± 13.1	0.15
β-OH-butyrate, mg/dl	9.08 ± 0.39	9.47 ± 0.23	0.07
Cholesterol, mg/dl	287.3 ± 33.7	205.9 ± 76.2	0.06
Bilirubin	0.61 ± 0.20	0.59 ± 0.49	0.93
AST, U/l	38.3 ± 3.67	37.1 ± 3.09	0.29
Total bile, μM	17.8 ± 7.04	17.3 ± 4.86	0.9

Values are means ± SD from 5 animals per group. Data were obtained from fasted mice during *week 6*, except total bile, which was measured in *week 12* of the high-fat diet. AAV, adeno-associated virus; SCR, scrambled; shRNA, short hairpin RNA; FATP2, fatty acid transport protein 2; HOMA-IR, homeostasis model assessment of insulin resistance; FFA, free fatty acid; TG, triglyceride; β-OH-butyrate, β-hydroxybutyrate; AST, aspartate aminotransferase. *Significant difference.

While the presence of FATP2 in peroxisomes has been confirmed, this is the first report that describes the quantification of the peroxisomal FATP2 population compared with the total pool of this protein in hepatocytes. On the basis of imaging analysis of FATP2 colocalization with peroxisome markers and Western blot experiments with immunopurified peroxisomes, >90% of FATP2 is outside liver peroxisomes. Using immunofluorescence and immunoelectron microscopy, we found that a significant fraction of the nonperoxisomal FATP2 is found on the plasma membrane, particularly in the space of Disse and in bile canaliculi.

The murine FATP2 sequence shares 34–50% amino acid identity with the other members of the murine FATP family and is most closely related to FATP6, a heart-specific protein that can enhance the uptake of LCFAs (11). Accordingly, FATP2 enhances LCFA uptake in mammalian cells (Fig. 2) and can compensate for the loss of the endogenous yeast FATP (5). This indicates that it is a bona fide fatty acid transporter. While FATP2-null mice have been reported previously (16), alterations in hepatic FFA uptake were not characterized. Thus we utilized an AAV-shRNA expression strategy, previously developed for targeting FATP5 (7), to specifically silence hepatic FATP2. We were able to efficiently suppress hepatic FATP2 expression in vivo without causing pathological alterations in serum aspartate aminotransferase or alanine aminotransferase levels, liver histology, or feeding behavior. AAV-shRNA expression affected only the target gene, FATP2, and not the related FATP4 or FATP5. As previously reported for

AAV8-based viruses (13), knockdown was liver-specific and did not affect the expression of FATP2 in the kidney. Thus the observed effects on whole body metabolism were most likely solely due to inhibition of hepatic FATP2.

Loss of FATP2 had a significant effect on hepatic FFA uptake, which, in many aspects, was similar to loss of FATP5. AAV-induced suppression of either protein resulted in a ~40% loss in the uptake (7). As diet-induced hepatosteatosis is at least in part mediated by the uptake of exogenous fatty acids by the liver, FATP2 function is likely to contribute to the disease etiology. We tested this hypothesis directly by eliminating FATP2 function subsequent to the establishment of hepatosteatosis. Despite unchanged food consumption, AAV-FATP2, but not AAV-SCR, transduction resulted in decreased total liver TG levels, a significant improvement in hepatocyte morphology, and decreased number and size of intracellular lipid droplets. Since absorption of fatty acids was unaffected by FATP2 knockdown, it was surprising that fat pad size was reduced and body weight was marginally improved. Together with the slight increase in lipid content of skeletal and cardiac muscle, this indicates that fatty acids not taken up by the liver were redirected to sites other than white adipocyte storage depots and, probably, metabolized. Clearly, further studies into changes in energy balance and metabolic rates following loss of FATP2 are needed.

Hepatosteatosis is closely linked to obesity-induced insulin resistance (14), and blocking FATP2 function may therefore improve insulin sensitivity. Indeed, starting at 4 wk postinjection, we observed significantly lower serum glucose levels in FATP2 knockdown than control mice. At the end of the 12-wk study, fasting glucose and insulin levels were significantly lower in AAV-shRNA-FATP2-injected mice. This resulted in an improved homeostasis model assessment of insulin resistance score, which has been shown to closely correlate with direct measurements of whole body insulin resistance (17). Together, these findings suggest that inhibition of FATP2 may be a target for the management of diabetes.

In contrast to the effects on LCFA uptake, AAV-mediated knockdown of hepatic FATP2 had modest effects on (V)LACS activity in this organ. This is not surprising, as FATP3-5, long-chain acyl-CoA synthetases, and Bubblegum (BG1) are known to have redundant (V)LACS functions (8, 31, 35). We found that while overall reduction of VLACS and LACS activity was not significant, peroxisomal LACS and VLACS activity was reduced by 59% and 51%, respectively. Given that the majority of FATP2 resides outside peroxisomes, it is likely that FATP2 (V)LACS activity requires additional, peroxisome-specific, cofactors. ABCD1, also known as ALDP, could be this potential interaction with FATP2. This peroxisomal X-ALD-linked ABC family member has been shown to promote peroxisomal association of FATP2 (40) and to bind directly in yeast-based interaction assays to FATP2 (22). If and how such interactions influence the enzymatic activities associated with FATP2 remain to be investigated. Furthermore, our observations also indicate that FATP2 is not the sole (V)LACS in peroxisomes, raising the interesting question of which protein(s) mediates the residual 50% activity.

FATP2 has also been suggested to be involved in a critical step of cholesterol catabolism and bile acid synthesis. Cholesterol catabolism to bile acids is initiated via a classical (CYP7A1) or an alternative (CYP27A1) pathway in the endoplasmic reticulum. It is followed by sterol ring modifications, which occur in the endoplasmic reticulum and cytoplasm, and side chain oxidation. Side chain oxidation is started by oxidation of a methyl group to carboxylic acid in mitochondria. Subsequently, activation of DHCA and THCA by a bile acid CoA synthetase is followed by side chain oxidation/shortening and amino acid conjugation in peroxisomes (28). FATP2 expression has been linked to activation of DHCA and THCA (23). Thus loss of the hepatic dihydroxycholestanoyl/trihydroxycholestanoyl-CoA synthetase function should lead to decreased bile and increased liver cholesterol levels. However, after knockdown of hepatic FATP2, we found no change in bile levels and no accumulation of hepatic total cholesterol or total cholesterol esters. While further experiments are needed for a more detailed examination of total bile composition, this indicates that FATP2 is not critical for DHCA/THCA activation and bile synthesis in vivo.

In a comparison of FATP2 with FATP5, some similarities and some differences arise. The knockdown of both genes leads to improvements in NAFLD and metabolic parameters. Although FATP2 and FATP5 account for a large portion of hepatic fatty acid uptake, the FATP5 knockdowns had a more profound effect on liver TG accumulation, diabetes, and weight loss. This more dramatic effect may be due to the suppressed appetite of the FATP5 knockdown mice (7). Redundant hepatic fatty acid uptake and (V)LACS activities of FATP2 and FATP5 may be distinguished by their expression patterns: FATP5 is restricted to the plasma membrane facing the space of Disse (6), while FATP2 is also expressed in the bile canaliculi and peroxisomes. This compartmentalization allows for different functions and roles in hepatocytes. Also, it is clear that FATP5 is responsible for the reconjugation of bile acids (19), but the role of FATP2 in bile synthesis requires more studies. Whether FATP2 or FATP5 is a better treatment target, in addition to any additive effects of knocking down both proteins, remains to be determined.

Overall, we have shown that FATP2 is a multifunctional protein, and its specific function may be dictated by its intracellular localization and organelle-specific interactions. Importantly, inhibition of FATP2 function leads to improved hepatosteatosis and insulin sensitivity. Targeting FATPs has recently become more attractive, as potent small-molecule inhibitors for human FATP2 (29) and FATP4 (3) have been identified in high-throughput compound screens, and pursuing hypomorphic modulation strategies of FATPs may lead to novel treatment options for obesity-related disorder.

GRANTS

This work was supported by American Dietetic Association Grants 7-07-MI-03 and 7-04-CD-14 to A. Falcon and A. Stahl, respectively, as well as National Institute of Diabetes and Digestive and Kidney Diseases Grant R01 DK-066336 to A. Stahl.

REFERENCES

1. **Ahlemeyer B, Neubert I, Kovacs WJ, Baumgart-Vogt E.** Differential expression of peroxisomal matrix and membrane proteins during postnatal development of mouse brain. *J Comp Neurol* 505: 1–17, 2007.
2. **Berger J, Truppe C, Neumann H, Forss-Petter S.** A novel relative of the very-long-chain acyl-CoA synthetase and fatty acid transporter protein genes with a distinct expression pattern. *Biochem Biophys Res Commun* 247: 255–260, 1998.
3. **Blackburn C, Guan B, Brown J, Cullis C, Condon SM, Jenkins TJ, Peluso S, Ye Y, Gimeno RE, Punreddy S, Sun Y, Wu H, Hubbard B,**

Kaushik V, Tummino P, Sanchetti P, Yu Sun D, Daniels T, Tozzo E, Balani SK, Raman P. Identification and characterization of 4-aryl-3,4-dihydropyrimidin-2(1H)-ones as inhibitors of the fatty acid transporter FATP4. *Bioorg Med Chem Lett* 16: 3504–3509, 2006.

4. **Brunt EM, Janney CG, Di Bisceglie AM, Neuschwander-Tetri BA, Bacon BR.** Nonalcoholic steatohepatitis: a proposal for grading and staging the histological lesions. *Am J Gastroenterol* 94: 2467–2474, 1999.
5. **DiRusso CC, Li H, Darwis D, Watkins PA, Berger J, Black PN.** Comparative biochemical studies of the murine fatty acid transport proteins (FATP) expressed in yeast. *J Biol Chem* 280: 16829–16837, 2005.
6. **Doege H, Baillie RA, Ortegon AM, Tsang B, Wu Q, Punreddy S, Hirsch D, Watson N, Gimeno RE, Stahl A.** Targeted deletion of FATP5 reveals multiple functions in liver metabolism: alterations in hepatic lipid homeostasis. *Gastroenterology* 130: 1245–1258, 2006.
7. **Doege H, Grimm D, Falcon A, Tsang B, Storm TA, Xu H, Ortegon AM, Kazantzis M, Kay MA, Stahl A.** Silencing of hepatic fatty acid transporter protein 5 in vivo reverses diet-induced non-alcoholic fatty liver disease and improves hyperglycemia. *J Biol Chem* 283: 22186–22192, 2008.
8. **Doege H, Stahl A.** Protein-mediated fatty acid uptake: novel insights from in vivo models. *Physiology (Bethesda)* 21: 259–268, 2006.
9. **Ferdinandusse S, Denis S, Dacremont G, Wanders RJ.** Toxicity of peroxisomal C_{27}-bile acid intermediates. *Mol Genet Metab* 96: 121–128, 2009.
10. **Folch J, Lees M, Sloane Stanley GH.** A simple method for the isolation and purification of total lipides from animal tissues. *J Biol Chem* 226: 497–509, 1957.
11. **Gimeno RE, Ortegon AM, Patel S, Punreddy S, Ge P, Sun Y, Lodish HF, Stahl A.** Characterization of a heart-specific fatty acid transport protein. *J Biol Chem* 278: 16039–16044, 2003.
12. **Grimm D, Kay MA, Kleinschmidt JA.** Helper virus-free, optically controllable, and two-plasmid-based production of adeno-associated virus vectors of serotypes 1 to 6. *Mol Ther* 7: 839–850, 2003.
13. **Grimm D, Streetz KL, Jopling CL, Storm TA, Pandey K, Davis CR, Marion P, Salazar F, Kay MA.** Fatality in mice due to oversaturation of cellular microRNA/short hairpin RNA pathways. *Nature* 441: 537–541, 2006.
14. **Harrison SA, Diehl AM.** Fat and the liver—a molecular overview. *Semin Gastrointest Dis* 13: 3–16, 2002.
15. **Hashmi M, Stanley W, Singh I.** Lignoceroyl-CoASH ligase: enzyme defect in fatty acid β-X-linked childhood adrenoleukodystrophy. *FEBS Lett* 196: 247–250, 1986.
16. **Heinzer AK, Watkins PA, Lu JF, Kemp S, Moser AB, Li YY, Mihalik S, Powers JM, Smith KD.** A very long-chain acyl-CoA synthetase-deficient mouse and its relevance to X-linked adrenoleukodystrophy. *Hum Mol Genet* 12: 1145–1154, 2003.
17. **Hermans MP, Levy JC, Morris RJ, Turner RC.** Comparison of tests of beta-cell function across from normal to diabetes. *Diabetes* 48: 1779–1786, 1999.
18. **Hirsch D, Stahl A, Lodish HF.** A family of fatty acid transporters conserved from *Mycobacterium* to man. *Proc Natl Acad Sci USA* 95: 8625–8629, 1998.
19. **Hubbard B, Doege H, Punreddy S, Wu H, Huang X, Kaushik VK, Mozell RL, Byrnes JJ, Stricker-Krongrad A, Chou CJ, Tartaglia LA, Lodish HF, Stahl A, Gimeno RE.** Mice deleted for fatty acid transport protein 5 have defective bile acid conjugation and are protected from obesity. *Gastroenterology* 130: 1259–1269, 2006.
20. **Liao J, Sportsman R, Harris J, Stahl A.** Real-time quantification of fatty acid uptake using a novel fluorescence assay. *J Lipid Res* 46: 597–602, 2005.
21. **Luers GH, Hartig R, Mohr H, Hausmann M, Fahimi HD, Cremer C, Volkl A.** Immuno-isolation of highly purified peroxisomes using magnetic beads and continuous immunomagnetic sorting. *Electrophoresis* 19: 1205–1210, 1998.
22. **Makkar RS, Contreras MA, Paintlia AS, Smith BT, Haq E, Singh I.** Molecular organization of peroxisomal enzymes: protein-protein interactions in the membrane and in the matrix. *Arch Biochem Biophys* 451: 128–140, 2006.
23. **Mihalik SJ, Steinberg SJ, Pei Z, Park J, Kim do G, Heinzer AK, Dacremont G, Wanders RJ, Cuebas DA, Smith KD, Watkins PA.** Participation of two members of the very long-chain acyl-CoA synthetase family in bile acid synthesis and recycling. *J Biol Chem* 277: 24771–24779, 2002.
24. **Moser HW.** Adrenoleukodystrophy: phenotype, genetics, and pathogenesis. *Brain* 120: 1485–1508, 1997.
25. **Mosser J, Douar AM, Sarde CO, Kioschis P, Feil R, Moser H, Poustka AM, Mandel JL, Aubourg P.** Putative X-linked adrenoleukodystrophy gene shares unexpected transporters. *Nature* 361: 726–730, 1993.
26. **Nakai H, Fuess S, Storm TA, Muramatsu S, Nara Y, Kay MA.** Unrestricted hepatocyte transduction with adeno-associated virus serotype 8 vectors in mice. *J Virol* 79: 214–224, 2005.
27. **Reynolds A, Leake D, Boese Q, Scaringe S, Marshall WS, Khvorova A.** Rational siRNA design for RNA interference. *Nat Biotechnol* 22: 326–330, 2004.
28. **Russell DW.** The enzymes, regulation, and genetics of bile acid synthesis. *Annu Rev Biochem* 72: 137–174, 2003.
29. **Sandoval A, Chokshi A, Jesch ED, Black PN, Dirusso CC.** Identification and characterization of small compound inhibitors of human FATP2. *Biochem Pharmacol* 79: 990–999, 2010.
30. **Schaffer JE, Lodish HF.** Expression cloning and characterization of a novel adipocyte long chain fatty acid transport protein. *Cell* 79: 427–436, 1994.
31. **Soupene E, Kuypers FA.** Mammalian long-chain acyl-CoA synthetases. *Exp Biol Med (Maywood)* 233: 507–521, 2008.
32. **Stahl A.** A current review of fatty acid transport proteins (SLC27). *Pflügers Arch* 447: 722–727, 2004.
33. **Stahl A, Gimeno RE, Tartaglia LA, Lodish HF.** Fatty acid transport proteins: a current view of a growing family. *Trends Endocrinol Metab* 12: 266–273, 2001.
34. **Stahl A, Hirsch DJ, Gimeno RE, Punreddy S, Ge P, Watson N, Patel S, Kotler M, Raimondi A, Tartaglia LA, Lodish HF.** Identification of the major intestinal fatty acid transport protein. *Mol Cell* 4: 299–308, 1999.
35. **Steinberg SJ, Morgenthaler J, Heinzer AK, Smith KD, Watkins PA.** Very long-chain acyl-CoA synthetases. Human "bubblegum" represents a new family of proteins capable of activating very long-chain fatty acids. *J Biol Chem* 275: 35162–35169, 2000.
36. **Steinberg SJ, Mihalik SJ, Kim DG, Cuebas DA, Watkins PA.** The human liver-specific homolog of very long-chain acyl-CoA synthetase is cholate:CoA ligase. *J Biol Chem* 275: 15605–15608, 2000.
37. **Steinberg SJ, Wang SJ, Kim DG, Mihalik SJ, Watkins PA.** Human very-long-chain acyl-CoA synthetase: cloning, topography, and relevance to branched-chain fatty acid metabolism. *Biochem Biophys Res Commun* 257: 615–621, 1999.
38. **Uchiyama A, Aoyama T, Kamijo K, Uchida Y, Kondo N, Orii T, Hashimoto T.** Molecular cloning of cDNA encoding rat very long-chain acyl-CoA synthetase. *J Biol Chem* 271: 30360–30365, 1996.
39. **Wanders RJ, van Roermund CW, van Wijland MJ, Schutgens RB, Schram AW, van den Bosch H, Tager JM.** Studies on the peroxisomal oxidation of palmitate and lignocerate in rat liver. *Biochim Biophys Acta* 919: 21–25, 1987.
40. **Yamada T, Taniwaki T, Shinnoh N, Uchiyama A, Shimozawa N, Ohyagi Y, Asahara H, Kira J.** Adrenoleukodystrophy protein enhances association of very long-chain acyl-coenzyme A synthetase with the peroxisome. *Neurology* 52: 614–616, 1999.
41. **Yokota S, Nagata T.** Ultrastructural localization of catalase on ultracryotomic sections of mouse liver by ferritin-conjugated antibody technique. *Histochemistry* 40: 165–174, 1974.
42. **Zou Z, DiRusso CC, Ctrnacta V, Black PN.** Fatty acid transport in *Saccharomyces cerevisiae*. Directed mutagenesis of FAT1 distinguishes the biochemical activities associated with Fat1p. *J Biol Chem* 277: 31062–31071, 2002.
43. **Zou Z, Tong F, Faergeman NJ, Borsting C, Black PN, DiRusso CC.** Vectorial acylation in *Saccharomyces cerevisiae*. Fat1p and fatty acyl-CoA synthetase are interacting components of a fatty acid import complex. *J Biol Chem* 278: 16414–16422, 2003.